Flow patterns and flow pattern map for liquid-liquid flow in a horizontal serpentine channel

Oguzhan Der, Kunle Olaitan, Volfango Bertola

University of Liverpool, School of Engineering, Laboratory of Technical Physics

Brownlow Hill, Liverpool, L69 3GH, United Kingdom

Volfango.Bertola@liverpool.ac.uk

Keywords: Liquid-liquid flow, Oil-water flow, Serpentine channel, Flow patterns

Abstract

The co-current oil-water flow in a horizontal serpentine channel is studied experimentally by high-speed imaging. Due to the channel geometry, the flow exhibits curved streamlines, which can induce secondary flows and alter the flow pattern transition boundaries in comparison with those observed in straight channels. This can have important applications in the development of microfluidic mixing devices. The serpentine channel was cut out in a black polypropylene sheet sandwiched between two transparent polypropylene sheets and bonded by selective laser welding. Different flow patterns were generated by changing independently the superficial velocities of the two fluids using a dual-drive syringe pump. Results enable the construction of a flow pattern map, which shows significant differences with the equivalent map obtained for straigt microchannels.

Introduction

Co-current flows of two immiscible liquids are common in food, pharmaceutical, personal and health care products, as well as in many industrial formulations. In particular, oil-water two-phase flows in microfluidic devices have been successfully employed in creating emulsions commonly used in the chemical and textile industries, food, and many other domains. In these applications, controlling the size distribution and polydispersity of the dispersed phase can improve significantly the characteristics of the final product (Tan et al. 2008).

Early studies on liquid-liquid flows focused mainly on oil-water systems in straight pipes of circular cross section, with diameters ranging between 1 cm and 10 cm (Brauner 2003). Later on, there was a growing interest in capillary tubes of millimetric diameter to investigate the flow behaviour in micro-gravity conditions (Beretta et al. 1997). More recently, investigations of the hydrodynamics and mass transfer aspects of liquid-liquid two phase flow have been extended to micro-channels with diameters < 1 mm, for their relevance in bio- and micro-fluidic applications (Burns & Ramshaw 2001; Kashid & Agar 2007). Experimental parameters include the inlet geometry (e.g. T-type and Y-type), the micro-channel cross-sections (e.g. square, rectangular and circular), flow rates and the flow ratio, and the physical properties of the fluids. The majority of works was limited to low flow velocities where surface forces dominate, in which intermittent flow patterns are generally observed.

The first step in the study of a liquid-liquid flow system requires the identification of flow patterns, which can be classified into four basic morphologies: (i) stratified layers with either smooth or wavy interface; (ii) large slugs, elongated or spherical, of one liquid in the other; (iii) a dispersion of relatively fine drops of one liquid in the other; (iv) annular flow, where one of the liquids forms the core and the other liquid flows in the annulus. In many cases, however, the flow pattern consists of a combination of these basic morphologies (Dessimoz et al. 2010). The identification of the flow pattern is usually based on visual observations, photographic/imaging techniques, or on abrupt changes in the average system pressure drop, sometimes combined with conductivity measurements or high frequency impedance probes for local holdup sampling, or local pressure fluctuations and average holdup measurements (Bertola 2003).

Oil-in-water flow patterns and slug hydrodynamics were experimentally studied in rectangular and square glass micro-channels of different hydraulic diameters ranging between 200 μm and 600 μm (Cao et al. 2018). The three main flow patterns observed were annular flow, slug flow and droplet flow, and general flow pattern transition criteria were proposed based on the Reynolds and the Weber numbers. In addition, a scaling law was proposed to predict the slug length, while the the slug velocity was shown to be a linear function of the bulk velocity of the two phases. Flow pattern maps for the same systems were produced as a function of the flow rates ratio and the Capillary number of the dispersed phase (Wu et al. 2017). Alternatively, flow pattern maps can be reported as a function of the Reynolds and the Capillary numbers (Kashid & Kiwi-Minsker 2011).

Experiments on liquid-liquid flow of different fluids in a square microchannel (200 μm hydraulic diameter) concluded that flow pattern maps based on Weber numbers cannot be generalised, and propose to introduce the product of the Weber and Ohnesorge numbers to as universal parameter to generalise flow maps (Yagodnitsyna et al. 2016).

Fluid mixing can be enhanced by fluid breakup in chaotic liquid-liquid flows (Muzzio et al. 1991). Chaotic fluid mixing can be obtained, for example, by means of secondary flow induced by curved streamlines (Castelain et al. 2001; Belkadi et al. 2011). Thus, one can build a simple, continuous flow chaotic mixer using a long serpentine channel. Adding complexity to the flow field has potential to increase the amount of mixing also in microchannels with zigzag geometry (Branebjerg et al. 1995) and three-dimensional serpentine channels designed to introduce chaotic advection into the system and further enhance mixing over a 2-D serpentine channel (Liu et al. 2000). Whilst these studies concern single-phase flows, the literature about liquid-liquid flows in serpentine or coiled channels is very limited (Sarkar et al. 2012; Wu & Sundén 2018).

The present work investigates experimentally the co-current oil-water flow in a polypropylene serpentine mini-channel of millimetric size with a square cross-section. Flow patterns were identified by high-speed imaging, and flow pattern maps were constructed with respect to different flow parameters and compared with those reported in the literature for straight channels.

Test section design and fabrication

The test section consisted of a polypropylene serpentine channel having a square cross section with a width $w = 3$ mm, consisting of a sequence of 46 circular half turns, with inner and outer radii of 1 mm and 4 mm, respectively, as shown in Figure 1a.

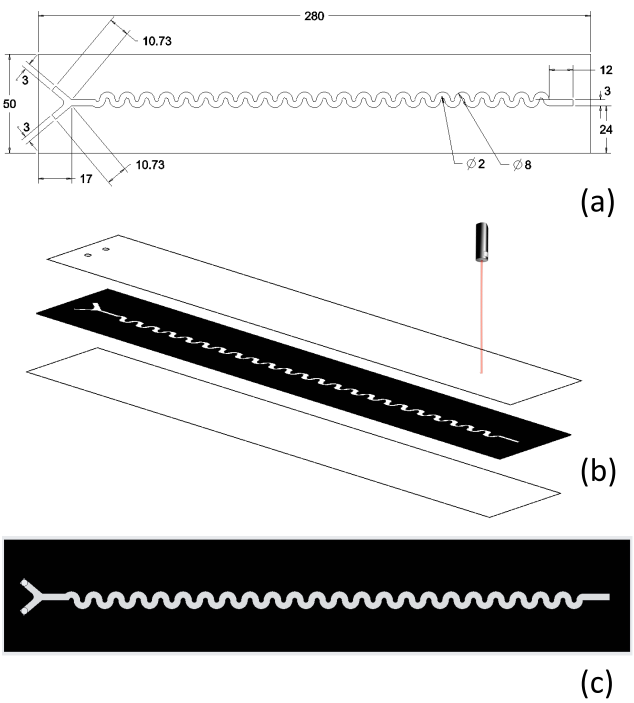

Figure 1: Schematic of the test section: (a) dimensions of the serpentine channel (in mm); (b) schematic of the laser welding process; (c) assembled test section.

The channel had two inlets, respectively for oil and water, merging together through a Y-junction, and one outlet. The channel shape was cut out into the black polypropylene sheet (3 mm thickness) using a LS1290 PRO Laser Cutter (maximum power: 80 W; cutting area: 1200 mm x 900 mm). The quality of the cut was determined mainly by the kerf width, which was kept as small as possible, and the roughness of the cut edge (Choudhury & Shirley 2010). To improve the cut edge finish, cutting was carried out repeating several engraving passes, removing approximately 0.1 mm of material at each pass. The surface of the cut polypropylene sheet was washed with an ethanol and distilled water to remove dust and impurities.

The channel was then sealed between two sheets of clear polypropylene (0.4 mm thickness each) by laser transmission welding (Amanat et al. 2010), using a nanosecond pulsed fibre laser (SPI G4 HS-L 20W) with a wavelength of 1064 nm and pulse repetition rate of 500 kHz. In this process, the laser beam goes through the clear transmissive layer and is absorbed by the adjacent black layer, melting the two sheets exactly at the interface (Humbe et al. 2014) as shown schematically in figure 1b.

Experimental setup and procedure

A schematic of the experimental layout is displayed in Figure 2. The two fluids (water and a commercial vegetable oil) were dispensed independently at controlled rate using a programmable syringe pump with dual drive system (Chemyx Fusion 4000). To minimise the transient inertial effects, the syringes were connected to the test section inlets by rigid nylon tubes.

For each fluid the flow rates, respectively $\dot{V}_o$ for oil and $\dot{V}_w$ for water, were varied between 0.5 mL/min and 5 mL/min, with increments of 0.5 mL/min; correspondingly, the superficial velocities, defined as $J_w = \dot{V}_w/L^2$ and $J_o = \dot{V}_o/L^2$ ranged between 0.926 mm/s and 9.26 mm/s.

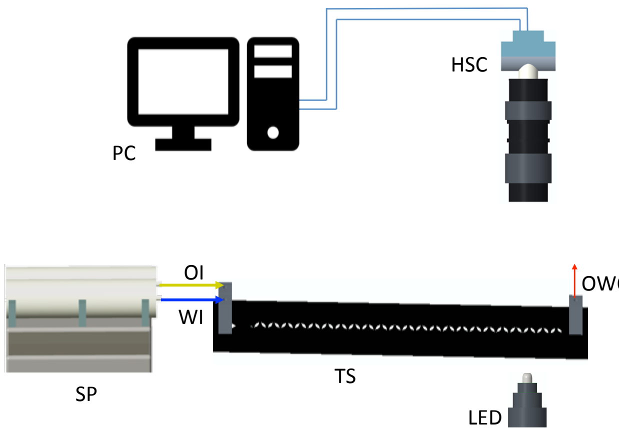

Figure 2: Schematic of the experimental setup displaying the two-channel syringe pump (SP), the test section with a water inlet (WI), an oil inlet (OI), and an oil-water outlet (OWO), the LED illumination system (LED), and the high-speed camera (HSC) connected to a computer equipped with frame grabber (PC).

Flow patterns were observed through the transparent walls of the channel using a high-speed CMOS camera (Mikrotron MC1310) placed above the channel, and equipped with a 18-108/2.5 zoom lens (Navitar Zoom 7000), with a resolution of 1280 x 440 pixels, at the rate of 200 frames per second. A single 3 W LED backlight equipped with diffuser was used to ensure uniform illumination and enhance the fluid interface contrast. The camera was placed at a distance from the inlet corresponding to 38 half-turns, i.e., 100 hydraulic diameters, to ensure the flow was fully developed.

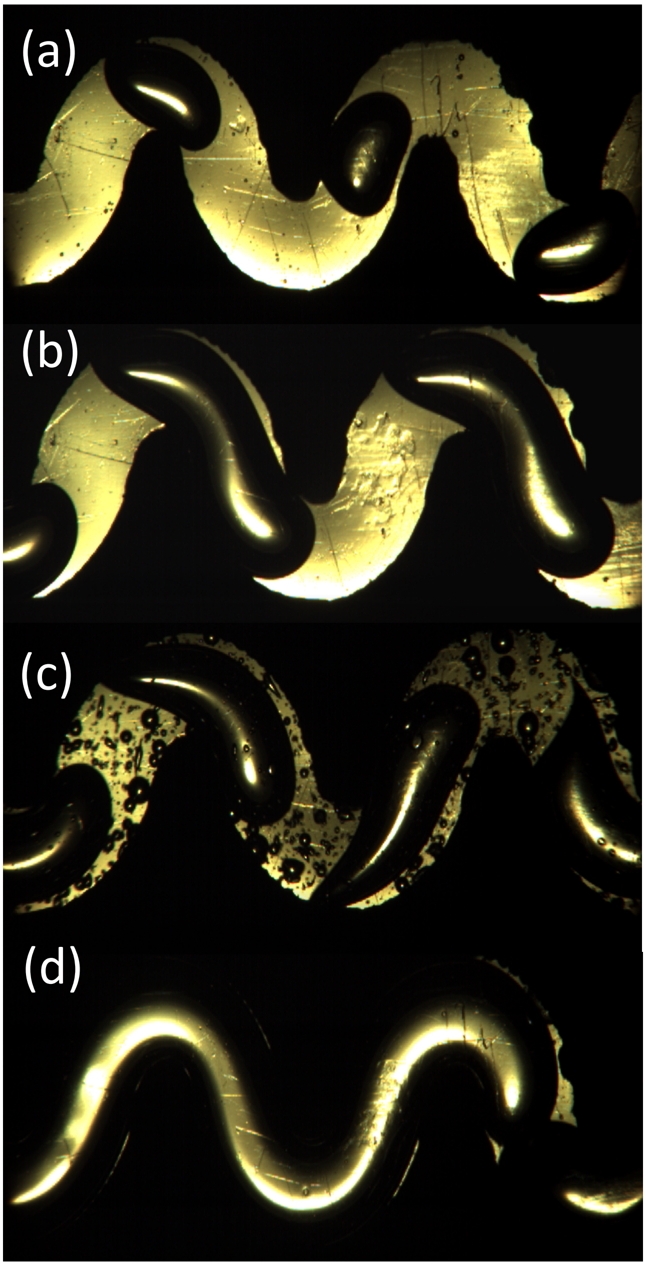

Figure 3: Flow patterns observed in the water-in-oil flow inside a serpentine channel with square cross-section (3 mm $\times$ 3 mm): (a) drop regime ($\dot{V}_W = 1$ ml/min, $\dot{V}_O = 3.5$ ml/min); (b) slug flow ($\dot{V}_W = 2$ ml/min, $\dot{V}_O = 2$ ml/min); (c) slug/dispersed flow ($\dot{V}_W = 3.5$ ml/min, $\dot{V}_O = 4$ ml/min); (d) slug/annular flow ($\dot{V}_W = 5$ ml/min, $\dot{V}_O = 2$ ml/min).

The fluid densities, measured by weighing a fixed volume of fluid with a precision analytical balance (Mettler Toledo), were $\rho_w = 998$ kg/m^3 and $\rho_o = 942$ kg/m^3 for water and oil, respectively. The fluid viscosities, measured with capillary viscometer (Schott Gerate) were $\eta_w = 1$ mPa·s and $\eta_o = 85$ mPa·s for water and oil, respectively. A Krüss EasyDyne tensiometer equipped with a Wilhelmy plate probe was used to measure the surface tensions of the two fluids, as well as their interfacial tension at the ambient temperature of 20°C. The fluid surface tensions were $\gamma_w = 72.8$ mN/m and $\gamma_o = 24.4$ mN/m for water and oil, respectively, while the interfacial tension was $\gamma_{wo} = 20.1$ mN/m. Correspondingly the capillary length, defined as:

$$a = \sqrt{\frac{\gamma_{wo}}{(\rho_w - \rho_o)\, g}} \tag{1}$$

was $a = 6.05$ mm, while the Eötvös number, defined as:

$$Eo = \frac{(\rho_w - \rho_o)\, g L^2}{\gamma_{wo}} \tag{2}$$

where $L = 3$ mm is the size of the channel cross section, was $Eo = 0.246$, which indicates that the interfacial tension dominates the flow.

The other relevant dimensionless parameters, i.e. the Reynolds number, the Weber number, and the Ohnesorge number, were calculated respectively as:

$$Re_{w,o} = \frac{\rho_{w,o} J_{w,o} L}{\eta_{w,o}} \tag{3}$$

$$We_{w,o} = \frac{\rho_{w,o} J^2_{w,o} L}{\gamma_{wo}} \tag{4}$$

$$Oh_{w,o} = \frac{\sqrt{We_{w,o}}}{Re_{w,o}} \tag{5}$$

Finally, the equilibrium contact angles of the two fluids on a polypropylene surface, measured from side views of sessile drops using a standard goniometer with digital image processing software (ImageJ), were $\theta_w = 50°$ and $\theta_o = 22°$ for water and oil, respectively.

Results

The typical flow patterns observed during the oil/water flow are displayed in Figure 3. Since the polypropylene channel walls are moderately hydrophobic ($\theta_W = 50°$), oil was the continuous phase in all the flow conditions considered (water-in-oil dispersion). In particular, four different flow patterns were identified:

- *Droplet flow* when the drops of the dispersed phase (water) have a size, measured along the curvilinear direction of the flow, $D_l \leq a$ (Figure 3a).
- *Slug flow* when the dispersed phase takes the form of elongated slugs, having a length measured along the curvilinear direction of the flow $D_l > a$ (Figure 3b).

- *Slug/dispersed flow* when the gap between consecutive slugs is a homogeneous dispersion of water droplets with a diameter $D \ll a$ (Figure 3c).

- *Slug/annular flow* when water flows in chains of very long slugs extending over several turns of the serpentine channel, separated from the channel walls by a thin oil film; the oil phase also fills the gap between the rounded tail and head of two consecutive slugs (Figure 3d).

The corresponding flow pattern maps are displayed in Figure 4; in particular, Figure 4a displays the map obtained using the superficial velocities of the two fluids as coordinates, while Figure 4b displays the same map using the dimensionless parameter $We \cdot Oh$ for the two phases as coordinates. This parameter arises from dimensional analysis arguments developed for the liquid-liquid flow in straight microchannels (Zhao et al. 2006; Yagodnitsyna et al. 2016).

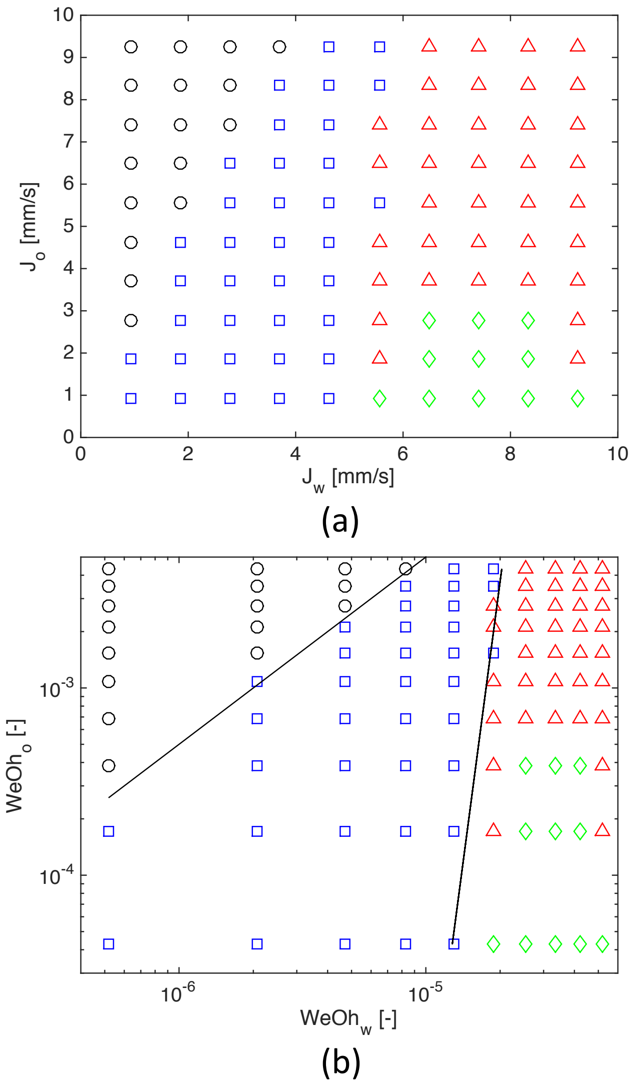

Figure 4: Flow pattern map for water-in-oil flow inside a serpentine channel with square cross-section (3 mm × 3 mm) plotted with respect to the superficial velocities of the fluids (a) and to the dimensionless variable WeOh (b); drop regime (○); slug flow (□); slug/dispersed flow (△); slug/annular (◇).

The solid lines in Figure 4b indicate the transition boundaries between the drop regime and the slug regime, and between the slug regime and the slug/dispersed regime, respectively. The transition boundary between the drop regime and the slug regime is well described by the following correlation:

$$(We \cdot Oh)_o = 500\,(We \cdot Oh)_w \tag{6}$$

while the transition boundary between the slug regime and the slug/dispersed regime is given by:

$$(We \cdot Oh)_w = 3.5 \cdot 10^{-5}\,(We \cdot Oh)_o^{0.1} \tag{7}$$

These results confirm the dimensional analysis arguments used to analyse flow pattern transition in straight channels are applicable to the serpentine geometry. However, the comparison with the universal flow pattern map for straight microchannels (Yagodnitsyna et al. 2016), displayed in Figure 5, reveals a significant difference. In particular, the transition between parallel flow and droplet flow in the universal flow pattern map corresponds to the transition between droplet flow and slug flow observed in the serpentine channel, and is shifted towards lower value of the parameter $We \cdot Oh$ of the continuous phase (oil in the present work).

A second difference is the absence of parallel flow in the serpentine channel, where it is replaced by three flow patterns: slug flow, slug/dispersed flow, and slug/annular flow, with the points corresponding to slug/annular flow located approximately in the centre of parallel flow region of the universal map. This suggests the secondary flow induced by curved streamlines enhances mixing of the two phases, by disrupting the stability of parallel flow and replacing it with intermittent flow patterns.

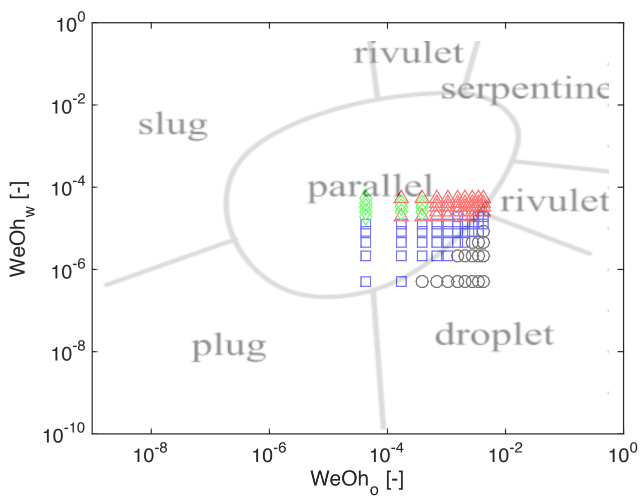

Figure 5: Comparison of results for water-in-oil flow inside a serpentine channel with square cross-section with the general flow pattern map plotted with respect to the dimensionless variable WeOh (Yagodnitsyna et al. 2016); drop regime (○); slug flow (□); slug/dispersed flow (△); slug/annular (◇).

The slug/annular flow, displayed in Figure 3d, is characterised by very long liquid slugs with only small amounts of oil between two consecutive slugs, therefore it could be regarded to as a pseudo-parallel flow regime. In this perspective, one can conclude the effect of the serpentine geometry is to shrink the region of parallel flow on the universal flow pattern map obtained for straight microchannels.

Figure 6 displays the dimensionless drop and slug length, D_l/L, plotted as a function of the superficial velocity of the continuous phase, J_o, for the different flow patterns observed. For $J_o \lesssim 4$ mm/s, the dimensionless length decreases for increasing J_o, while above $J_o \gtrsim 4$ mm/s it remains approximately constant and equal to the capillary length (Eq. 1).

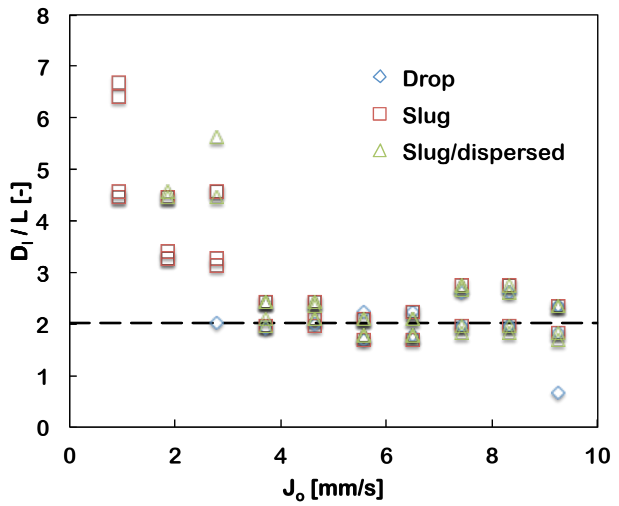

Figure 6: Slug and drop dimensionless length, D_l/L, as a function of the superficial velocity of the continuous phase (oil). The discontinuous horizontal line indicates the capillary length.

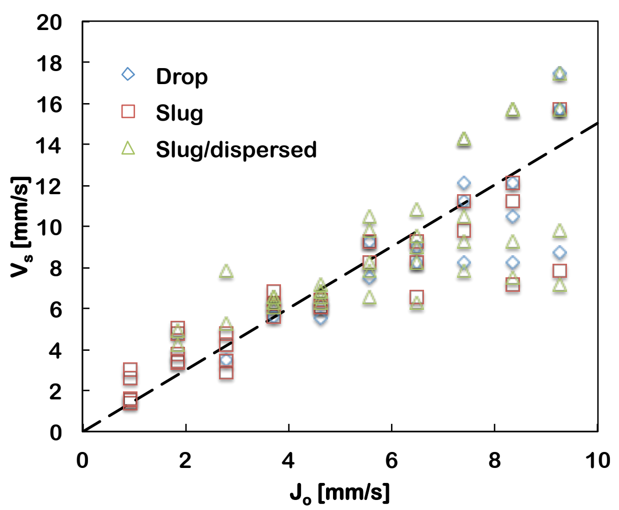

Figure 7: Slug and drop velocity as a function of the superficial velocity of the continuous phase (oil). The discontinuous line represents the linear correlation $V_s = 1.5 J_o$.

The slug and drop velocity, V_s, is approximately a linear function of the superficial velocity of the continuous phase, as shown in Figure 7, in agreement with the literature (Cao et al. 2018; Yagodnitsyna et al. 2016).

Conclusions

The two-phase flow of oil and water flow in a horizontal serpentine channel was investigated experimentally by high-speed imaging. Different flow regimes were identified depending on the superficial velocities of the two fluids, and sorted into an empirical flow pattern map. Flow pattern transitions were found to be a function of the product of the Weber and Ohnesorge numbers, in agreement with dimensional analysis arguments for straight channels.

The serpentine geometry enhances the fluids mixing with respect to straight channels, by reducing significantly the area of the separated flow region.

Finally, the slug length and velocity correlate with the superficial velocity of the continuous phase, irrespective of the flow pattern, and in agreement with the literature.

Acknowledgments

O. Der gratefully acknowledges a YLSY doctoral studentship from the Republic of Turkey, Ministry of National Education.

References

Tan, J., Xu, J.H., Li, S.W. & Luo, G.S. (2008) Drop dispenser in a cross-junction microfluidic device: Scaling and mechanism of break-up, Chemical Engineering Journal, Vol. 136, pp. 306–311.

Brauner, N. (2003) Liquid-Liquid Two-Phase Flow Systems, in Bertola, V. (Ed.) Modelling and Experimentation in Two-Phase Flow. Springer, New York.

Beretta, A., Ferrari, P., Galbiati, L., & Andreini, P.A. (1997) Oil-Water Flow in Small Diameter Tubes. Flow Patterns, International Comm. Heat Mass Transfer, Vol. 24, pp. 223–229.

Burns, J.R. & Ramshaw, C. (2001) The intensification of rapid reactions in multiphase systems using slug flow in capillaries, Lab on a Chip, Vol. 1, pp. 10–15.

Kashid, M.N. & Agar, D.W. (2007) Hydrodynamics of liquid-liquid slug flow capillary microreactor: flow regimes, slug size and pressure drop, Chemical Engineering Journal, Vol. 131, pp. 1–13.

Dessimoz, A.L., Raspail, P., Berguerand, C., & Kiwi-Minsker, L. (2007) Quantitative criteria to define flow patterns in micro-capillaries, Chemical Engineering Journal, Vol. 160, pp. 882–890.

Bertola, V. (2003) Experimental characterization of gas-liquid intermittent subregimes by phase density function measurements, Experiments in Fluids, Vol. 34, pp. 122–129.

Cao, Z., Wu, Z. & Sundén, B. (2018) Dimensionless analysis on liquid-liquid flow patterns and scaling law on slug hydrodynamics in cross-junction microchannels, Chemical Engineering Journal, Vol. 344, pp. 604–615.

Wu, Z., Cao, Z., & Sundén, B. (2017) Liquid-liquid flow patterns and slug hydrodynamics in square microchannels of cross-shaped junctions, Chemical Engineering Science, Vol. 164, pp. 56–66.

Kashid, M., & Kiwi-Minsker, L. (2007) Quantitative prediction of flow patterns in liquid-liquid flow in micro-capillaries, Chemical Engineering and Processing, Vol. 50, pp. 972–978.

Yagodnitsyna, A.A., Kovalev, A.V. & Bilsky, A.V. (2016), Flow patterns of immiscible liquid-liquid flow in a rectangular microchannel with T-junction, Chemical Engineering Journal, Vol. 303, pp. 547–554.

Muzzio, F.J., Tjahjadi, M. & Ottino, J.M. (1991), Self-similar drop-size distributions produced by breakup in chaotic flows, Physical Review Letters, Vol. 67, pp. 54–57.

Castelain, C., Mokrani, A., Le Guer, Y. & Peerhossaini, H. (2001), Experimental study of chaotic advection regime in a twisted duct flow, Eur. J. Mech. B-Fluids, Vol. 20, pp. 205–232.

Belkadi, A., Tarlet, D., Castelain, C., Bellettre, J. & Burghelea, T. (2011) Mesures in situ de l'écoulement secondaire d'un melangeur à advection chaotique, 14ème Congrès Francais de Visualisation et de Traitement d'Images en Mécanique des Fluides, Lille (France), 21–25 November 2011.

Branebjerg, J., Fabius, B., & Gravesen, P. (1995), Application of Miniature Analyzers: From Microfluidic Components to TAS, in A. van den Berg and P. Bergveld (Ed.), Micro Total Analysis Systems. Kluwer Academic Publishers, Dordrecht, pp 141–151.

Liu, R.H., Stremler, M.A., Sharp, K.V., Olsen, M.G., Santiago, J.G., Adrian, R.J., Aref, H., & Beebe, D.J. (2000) Passive Mixing in a Three-Dimensional Serpentine Microchannel, J. MEMS, Vol. 9, pp. 190–197.

Sarkar, P.S., Singh, K.K., Shenoy, K.T. Sinha, A. Rao, H. & Ghosh, S.K. (2012) Liquid-Liquid Two-Phase Flow Patterns in a Serpentine Microchannel, Ind. Eng. Chem. Res., Vol. 51, pp. 5056–5066.

Wu, Z. & Sundén, B. (2018), Liquid-liquid two-phase flow patterns in ultra-shallow straight and serpentine microchannels, Heat Mass Transfer, pp. 1–14.

Choudhury, I.A. & Shirley, S. (2010), Laser cutting of polymeric materials: An experimental investigation, Optics-Laser Technology, Vol. 42, pp. 503–508.

Amanat, N., James, N.L. & McKenzie, D.R. (2010) Welding methods for joining thermoplastic polymers for the hermetic enclosure of medical devices, Med. Eng. Phys., Vol. 32(7), pp. 690–699.

Humbe, A.B., Deshmukh, P.A., Jadhav, C.P. & Wadgane, S.R. (2014) Review of laser plastic welding process, International Journal of Research in Engineering - Technology, Vol. 2(2), pp. 191–206.

Zhao, Y., Chen, G. & Yuan (2006) Liquid-Liquid Two-Phase Flow Patterns in a Rectangular Microchannel, AIChE Journal, Vol. 52(12), pp. 4052–4060.